NJC

Accepted Manuscript

ROYAL SOCIETY OF CHEMISTRY

rsc.li/njc

View Article Online
DOI: 10.1039/C6NJ02507B

Journal Name

ARTICLE

Metal organic frameworks-derived Co_3O_4 microcubes and catalytic application in CO oxidation

Received 00th January 20xx,
Accepted 00th January 20xx

DOI: 10.1039/x0xx00000x

www.rsc.org/

Chi Zhang, Li Zhang,* Guan-Cheng Xu, Xin Ma, Ying-Hai Li, Chu-Yang Zhang, Dian-Zeng Jia*

Metal-organic frameworks (MOFs) derived metal oxides with diverse morphologies and microporous structures have shown potential application in heterogeneous catalysis. In this paper, two kinds of porous Co_3O_4 catalysts, Co_3O_4-MA and Co_3O_4-DMA (MA = methylamine and DMA = dimethylamine), have been successfully synthesized via one-step pyrolysis of Co-based metal-formate frameworks [Amine][$Co(HCOO)_3$] (Amine = methylamine, dimethylamine) under air. The obtained porous Co_3O_4 catalysts were systematically characterized by XRD, SEM, TEM, XPS, H_2-TPR and N_2 adsorption-desorption analysis. The results show that the obtained porous Co_3O_4 catalysts are composed of nanoparticles and inherit the morphology from the precursors [Amine][$Co(HCOO)_3$]. The Co_3O_4-MA and Co_3O_4-DMA exhibit excellent catalytic activity for CO oxidation, both of them reach 100% of CO conversion at 170 °C.

1. Introduction

Reducing CO concentration in the air by active catalysts and reaching the allowed concentration levels according to environmental regulations has become a top priority.[1] So the CO oxidation heterogeneous catalysis is an important research area which attracted more and more attention.

As the CO oxidation catalysts, noble metals possess high activity and desirable thermal stability, but the disadvantages of high cost and low availability make them compulsion to consider transition metal catalyst as an alternative.[2] Among the transition metal oxides, cobalt oxide is considered to be one of the most important transition metal catalysts which possesses excellent CO oxidation activity both at ambient temperature and lower temperature as -77 °C.[3] Much effort has been devoted to research the influence of the particle size and shape effect with regard to CO oxidation. Recent scientific researches have shown that the physical and chemical properties of Co_3O_4 are closely associated with the morphology and porosity.[4] Therefore, it is fundamental and technological interest to develop facile and efficient synthetic approaches for the preparation of specific porous and morphology-controlled Co_3O_4.

Since the last decade, metal-organic frameworks (MOFs) has attracted wide attention of researchers because of their potentialities and the unprecedented properties.[5,6] Owing to their open channels, permanent cavities and order crystalline lattice, MOFs have been used as hosts for the synthesis of the metal-oxide nanoparticles.[7] For example, Wang *et al.* employed ZIF-8 ($Zn(MeIM)_2$, MeIM=2-methylimidazole) as a host to prepare neat Co_3O_4 nanoparticles, which exhibit high specific rate 12.8 mmol g^{-1} h^{-1} at 70 °C, good cycling stability and long-term stability in CO oxidation.[8] Tan *et al.* used MIL-53(Al) with high thermal stability as a support material of a copper catalyst for CO oxidation.[9] Moreover, owing to their uniform and tridimensional structures within inorganic clusters connected by organic moieties,[10] which make MOFs good candidates in chemical sensors,[11] lithium ion batteries,[12] supercapacitor,[13] catalysis,[14] and so forth, various MOF-derived metal oxides and composites were synthesized and utilized as catalysts for CO oxidation which exhibit excellent catalytic activity. Recently, Zhang *et al.* employed Cu-based MOFs to prepare CuO/Cu_2O porous composites with adjustable composition and various morphologies, and the porous composites reach 100% of CO conversion at 240~260 °C.[15] Qin *et al.* prepared $AO_x/CuO_y/C$ (A = Sr, La, Ce, Al) composites by using A-Cu-BTC as precursor, and one of CuO_y/C showed the promising catalysts in selective catalytic reduction of NO with CO.[16] Yan *et al.* synthesized rattle-type $Co_3O_4@SiO_2$ nanoparticles via thermal decomposition of $Co_3[Co(CN)_6]_2@SiO_2$ core–shell nanocubes, which reaches 100% of CO conversion at 150 °C.[17] Wang *et al.* synthesized nanoscale Co/C by simple pyrolysis of a Co-containing metal-organic framework (ZIF-67) at 600 °C, which exhibited high catalytic activity for CO oxidation even at a temperature as low as -30 °C.[18] Pang *et al.* calcined the corresponding nanostructured Co-8-hydroxyquinoline coordination precursor in air and then obtained Co_3O_4 which can catalyze the oxidization of nearly 100% of CO to CO_2 at 100 °C.[19] However, facile and controlled synthesis of nanostructured porous

Key Laboratory of Energy Materials Chemistry (Xinjiang University), Ministry of Education. Key Laboratory of Advanced Functional Materials, Autonomous Region. Institute of Applied Chemistry, Xinjiang University, Urumqi, 830046, Xinjiang, P. R. China.
*Corresponding author. E-mail: zhanglixju@163.com, jdz0991@gmail.com Tel./Fax: +86-991-8580586

View Article Online
DOI: 10.1039/C6NJ02507B

Co_3O_4 catalysts derived from the thermolysis of Co-based MOFs is still in its infancy.

Herein, we report a facile strategy to prepare porous Co_3O_4 catalysts by calcining formate-based metal-organic frameworks. As various structure and shapes of metal-formate frameworks can be controlled to achieve by using ammonium cation templates,[20] the porous Co_3O_4 were prepared via simple solid-state thermolysis of the Co-based metal-formate frameworks. The as-made Co_3O_4 remain the shape of the precursors very well, and show excellent catalytic for CO oxidation. The results indicates the synergy of O_v, O_c and Co^{3+} sites is considered to be the main effect on catalytic activity of Co_3O_4 for CO oxidation and the specific surface area seemed less important. This method is also applicable to the preparation of other metal oxides with a number of potential applications.

2. Experimental details

All the chemical reagents were purchased commercially and used without further purification.

2.1 Synthesis of [Amine][Co(HCOO)$_3$] (Amine = NH_3CH_3, $(CH_3)_2NH_2$)

In a typical synthesis, 2.38 g of $CoCl_2 \cdot 6H_2O$ and 1 g of PVP were dissolved in 20 mL of methanol in a beaker. 3.106 g of methylamine water solution (NH_2CH_3, 40%), 2.7618 g of formic acid (HCOOH, 88%) and 1 g of PVP were dissolved in 20 mL of methanol. Then the cobalt chloride solution was dropped into the ligand solution. The mixture was stirred at room temperature for 30 minutes and aged for 30 minutes. The resulting pink precipitates were collected by centrifugation-redispersion cycles to remove any possible residual reactants, and finally dried under vacuum at 40 ^oC for 5 h.

In the preparation of $[(CH_3)_2NH_2][Co(HCOO)_3]$, methylamine water solution were replaced by 5.464 g dimethylamine water solution ($(CH_3)_2NH$, 33%) and similar procedure was used.

2.2 Synthesis of porous Co_3O_4 catalysts

Co_3O_4 catalysts were obtained from calcination of [Amine][Co(HCOO)$_3$]. Thermal decomposition was achieved under air in a muffle furnace with a heating rate of 1 K min^{-1} up to 500 ^oC and maintained for 2 h. The two samples were named as Co_3O_4-MA and Co_3O_4-DMA, respectively.

For purposes of comparison, commercial Co_3O_4, donated as Co_3O_4-C, was purchased from a commercially available source (Tianjin Kwangfu).

2.3 Material characterizations

Thermogravimetric analyses (TGA) were performed on a Netzsch SDT449F3 thermal analyzer in air atmosphere at a scan rate of 10 K min^{-1}. Scanning electron microscope (SEM) images were taken using a Hitachi S-4800 microscope. Transmission electron microscopy (TEM) images were obtained with a Hitachi H600 microscope. Powder X-ray diffraction (XRD) data were recorded on a Bruker D8 advance diffractometer at 40 KV and 40 mA using Cu Kα radiation (λ = 0.15405 nm) radiation, with a step size of 0.02^o in 2θ. The surface area and N_2 adsorption-desorption isotherm measurement were carried out on a Micromeritics ASAP 2020 analyzer at 77 K. Prior to the measurement, the sample was degassed at 120 ^oC for 6 h in the vacuum line. X-ray photoelectron spectroscopy (XPS) was performed on an Escalab 250 Xi from Thermo Fisher Scientific. H_2 temperature-programmed reduction (H_2-TPR) analysis was performed by using a Micromeritics Chemisorb 2920 apparatus. For each analysis, accurate amounts of calcined sample (60~65 mg) were purged in a flow of pure argon at 200 ^oC for 120 min to remove traces water (heating rate 10 ^oC /min). After cooling to room temperature, H_2-TPR experiments were performed using a 10 vol% H_2 /Ar mixture at a flow rate of 50 mL/min. The sample was heated from ambient temperature to 800 ^oC at heating rate of 10 ^oC /min and H_2 consumption was detected by a thermal conductivity detector (TCD).

2.4 Catalytic performance test

50 mg catalysts were put in a quartz glass reaction tube without any pre-treatment. The reaction temperature was monitored by a thermocouple placed in the middle of the catalyst bed. A mixture of 1 vol % CO and 20 vol % O_2 balanced by N_2 was introduced as the reactants. The total flow rate was 50 mL min^{-1}, corresponding to a space velocity of 60000 mL g^{-1} h^{-1}. Online analysis of CO and CO_2 was performed at each temperature after a stabilization time of about 20 min with Agilent GC7890 gas chromatograph. The CO conversion was calculated based on the change in CO concentrations of the inlet and outlet gases as follow:

$$R_{CO} = \left(1 - \frac{|CO|_{OUT}}{|CO|_{IN}}\right) \times 100\%$$

3. Results and discussion

Metal-formate frameworks were used as precursors in this work. Templated by ammonium cations, two metal-formate frameworks [Amine][Co(HCOO)$_3$] (Amine = NH_3CH_3, $(CH_3)_2NH_2$) were formed.[21, 22] A modified precipitation method was used in this work to obtain the microcrystals of two metal-formate frameworks. Cobalt chloride, formic acid neutralized by amines frameworks. Cobalt

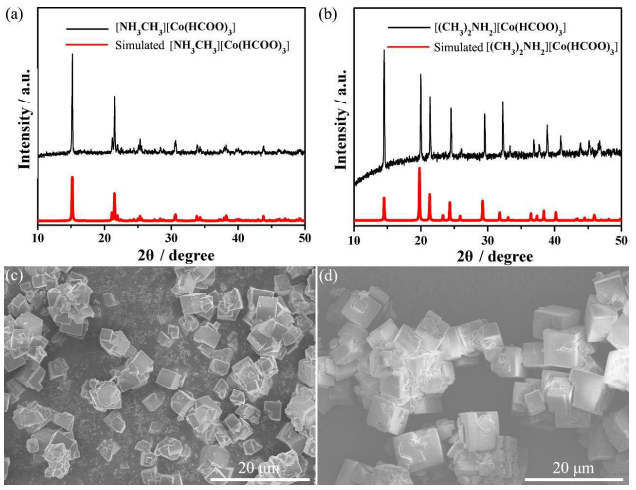

Fig. 1 XRD patterns (a, b) and SEM (c, d) images of $[NH_3CH_3][Co(HCOO)_3]$ (a, c), and $[(CH_3)_2NH_2][Co(HCOO)_3]$ (b, d).

View Article Online
DOI: 10.1039/C6NJ02507B

chloride, formic acid neutralized by amines and PVP were used as the reactants, and the whole synthesizing process was run mildly at ambient temperature. The polymer PVP was added as an additive in the crystallization to tune the size of the resulting crystals. XRD patterns of the as-prepared samples, as shown in Fig. 1a-b, match well with the simulated XRD patterns,[21, 22] indicating the formation of pure phase $[NH_3CH_3][Co(HCOO)_3]$ and $[(CH_3)_2NH_2][Co(HCOO)_3]$. SEM images (Fig. 1c-d) show that the as prepared $[NH_3CH_3][Co(HCOO)_3]$ and $[(CH_3)_2NH_2][Co(HCOO)_3]$ are consisted of microcubes, and the size distribution are about 5 μm and 7 μm, respectively.

The thermal behaviour of the $[Amine][Co(HCOO)_3]$ in air are shown in Fig. 2a. The curves indicate two-step weight-loss patterns of the compounds. The first weight losses are ascribed to the removal of amine and one formate molecule per formula unit. The second losses are attributed to the decomposition of remaining organic components. The final residues were found to be 35.9% and 36.3%, which are close to the calculated values of 35.4% and 33.5%, estimated as Co_3O_4 produced from $[NH_3CH_3][Co(HCOO)_3]$ and $[(CH_3)_2NH_2][Co(HCOO)_3]$, respectively. Based on the TG results, we predicted that Co_3O_4 could be formed by pyrolyzation of $[NH_3CH_3][Co(HCOO)_3]$ and $[(CH_3)_2NH_2][Co(HCOO)_3]$ at temperature higher than 350 °C. Therefore, the as-prepared $[NH_3CH_3][Co(HCOO)_3]$ and $[(CH_3)_2NH_2][Co(HCOO)_3]$ were annealed at 500 °C for 2 h, and Co_3O_4-MA and Co_3O_4-DMA were obtained. XRD results of Co_3O_4-MA and Co_3O_4-DMA are shown in Fig. 2b. The peaks at 2θ = 18.9°, 31.2°, 36.8°, 38.5°, 44.8°, 55.3°, 59.3°, and 65.2° correspond well to the characteristic (111), (220), (311), (222),

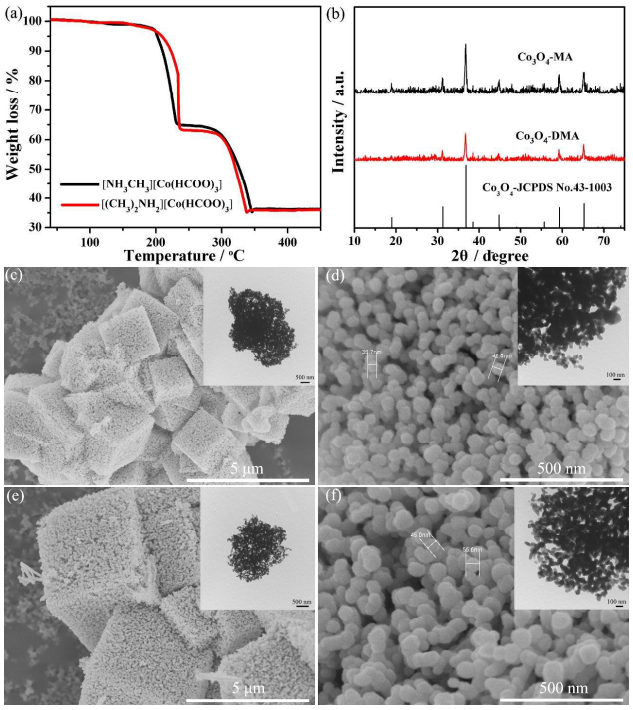

Fig. 2 (a) TGA curves of the as-synthesized $[NH_3CH_3][Co(HCOO)_3]$ and $[(CH_3)_2NH_2][Co(HCOO)_3]$ microcrystals in air flow; (b) XRD patterns of the Co_3O_4 products obtained from calcination of the as-prepared precursors in air; SEM images with insets showing TEM images of (c, d) Co_3O_4-MA and (e, f) Co_3O_4-DMA.

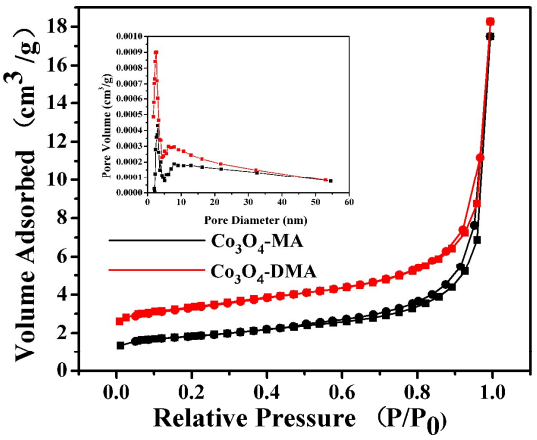

Fig. 3 Adsorption and desorption isotherms for nitrogen (at 77 K) of the Co_3O_4-MA (black) and Co_3O_4-DMA (red). Inset shows the corresponding Barrett-Joyner-Halenda (BJH) pore size distribution.

(400), (422), (511), and (440) reflections of Co_3O_4 (JCPDS No. 43-1003), respectively. Moreover, the sharp diffraction peaks confirm the high crystallinity of Co_3O_4-MA and Co_3O_4-DMA. More structural information was revealed by SEM and TEM. SEM images (Fig. 2c-f) show that the obtained Co_3O_4-MA and Co_3O_4-DMA retain the geometries of the precursors with smaller size about 3 μm and 5 μm, respectively. Moreover, the Co_3O_4-MA and Co_3O_4-DMA microcubes are composed of nanoparticles with size distributions about 35 ~ 42 nm and 45 ~ 70 nm, respectively. There are a lot of pores distributed on the surface of cobalt oxides. In addition, the interior structure of Co_3O_4-MA and Co_3O_4-DMA was further studied by TEM. TEM images, as shown in Fig. 2c-f insets, reveal that the interior structures are composed of nanoparticles and abundant pores, which might ascribed to the gas released during the process of thermal decomposition of the precursors.

The N_2 adsorption−desorption isotherm curves are shown in Fig. 3. It can be seen that both of the samples exhibit type-IV adsorption isotherms with a clear hysteresis loop, indicating the presence of mesoporous structure in the samples. The Barrett-Joyner-Halenda (BJH) pore size distribution curves in the inset of Fig. 3 shows the pore size distributions of Co_3O_4-MA and Co_3O_4-DMA are in the similarity mesoporous range (2.3~5 nm). The specific surface areas of Co_3O_4-MA and Co_3O_4-DMA calculated through Brunauer–Emmett-Teller (BET) method were 6.77 m^2/g and 9.37 m^2/g, respectively. The comparatively low specific surface areas might be due to the excessive pyrolysis make the particles aggregating.

Attempts were made to investigate the catalytic activities of the as-obtained Co_3O_4 catalysts for CO oxidation. The reactions were carried out in a fixed-bed flow reactor with 50 mg catalysts and with a gas flow mixed of CO (0.5 ml min^{-1}), O_2 (10 ml min^{-1}), and N_2 (39.5 ml min^{-1}). The catalytic activity for CO oxidation as a function of the temperature is shown in Fig. 4a. Apparently, the synthesized Co_3O_4-DMA catalyst exhibits the best catalytic activity for CO oxidation. The T_{50} (the temperature of 50% conversion) for Co_3O_4-DMA is 160 °C, which is 3 °C lower than that of Co_3O_4-MA (T_{50}=163 °C). The temperatures for 100% CO conversion of Co_3O_4-MA and Co_3O_4-DMA are both at 170 °C. In contrast, Co_3O_4-C shows poor CO oxidation activity with T_{50} at 230 °C and only 75%

View Article Online
DOI: 10.1039/C6NJ02507B

CO conversion was obtained even when the temperature reaches highly at 320 °C. These results demonstrate that the porous Co_3O_4 prepared in this work can effectively catalyze the CO oxidation at a lower temperature, and the full CO conversion temperature is much lower than that of Co_3O_4-C. The better catalytic properties of Co_3O_4-MA and Co_3O_4-DMA might be attributed to their small particles and porous structures, which offer a larger contact area with CO. The Arrhenius plots of CO oxidation over the two samples are shown in Fig. 4b. The apparent activation energy (kJ mol^{-1}) was calculated using conversion data between 130 °C and 170 °C. The apparent activation energy of CO oxidation over Co_3O_4-MA and Co_3O_4-DMA are 155.4 kJ mol^{-1} and 113.2 kJ mol^{-1}, respectively. Thus, Co_3O_4-DMA shows a better catalytic activity than Co_3O_4-MA due to its lower value of activation energy of CO oxidation. Furthermore, cycling tests were performed to study the stability of Co_3O_4-MA and Co_3O_4-DMA, as shown in Fig. 4c-d, and no significant deactivations were observed in the second run. Moreover, the catalytic durability of Co_3O_4-MA and Co_3O_4-DMA was also evaluated at 180 °C under the similar conditions (Fig. 4e). It is found that there is no decay of CO conversion even after 20 h. Therefore, the two porous Co_3O_4 catalysts, Co_3O_4-MA and Co_3O_4-DMA, prepared via one-step pyrolysis of Co-based metal-organic frameworks, exhibit good cycling and long-term stability of CO oxidation.

As the CO oxidation is always dependent on the redox properties of catalysts, H_2-TPR analyses were performed to investigate the redox behavior. As shown in Fig. 4f, the reduction of Co_3O_4 follows the following steps: $Co_3O_4 \rightarrow CoO \rightarrow Co$.[23] Both of the reduction of Co_3O_4-MA and Co_3O_4-DMA started at 200 °C. Co_3O_4-DMA exhibits only one peak at 375 °C, while Co_3O_4-MA presents two peaks at 391 °C and 448 °C, assigned to the chemisorbed/dissociated oxygen and bulk-phase lattice oxygen, respectively. This observation can be explained by the particle size of Co_3O_4, of which the larger particles of Co_3O_4-DMA are usually reduced to metallic cobalt in one step.[24] In addition, Co_3O_4-DMA shows lower reduction temperature and higher hydrogen consumption between 200 °C and 350 °C, suggesting that Co_3O_4-DMA is more likely to be reduced than Co_3O_4-MA.

Many works have been done to study the mechanisms of catalytic activity of Co_3O_4 for CO oxidation.[3,25-27] The mechanism of CO oxidation could proceed as below:

$$1/2\ O_2 + X \leftrightarrow O \cdot X \quad (1)$$

$$CO + O \cdot X \leftrightarrow CO_2 \cdot X \quad (2)$$

$$CO_2 \cdot X \leftrightarrow CO_2 + X \quad (3)$$

where "X" denotes the active site. The adsorption of oxygen occurs at the active site (Eq. (1)) and the CO is oxidized by chemisorbed and dissociated oxygen species (Eq. (2)).[26] CO and surface O_2 molecules chemisorbs preferably at a surface-exposed Co^{3+} site, and then the CO is oxidized by surface oxygen resulting oxygen vacancy subsequently.[3,27] Therefore, the active site is widely considered to be the major factor of the catalytic activity in CO oxidation. In addition, the chemisorbed oxygen and oxygen vacancies may also be active for oxygen exchange and CO oxidation.

As can be seen from above the results, both of the two catalysts are with small BET surface areas, but exhibit excellent CO oxidation performance. We predict that the BET surface area does not play the leading role in CO oxidation in this study. Therefore, the probable catalytic mechanisms should be further discussed. XPS analysis was performed to investigate the chemical state of the elements present in Co_3O_4-MA and Co_3O_4-DMA as well as to understand the influence of the Co^{3+} and oxygen components. As shown in Fig. 5a-b, the sharp peaks at 780.1, 530.4, 284.9 eV correspond to the characteristic peaks of Co 2p, O 1s, and C 1s,

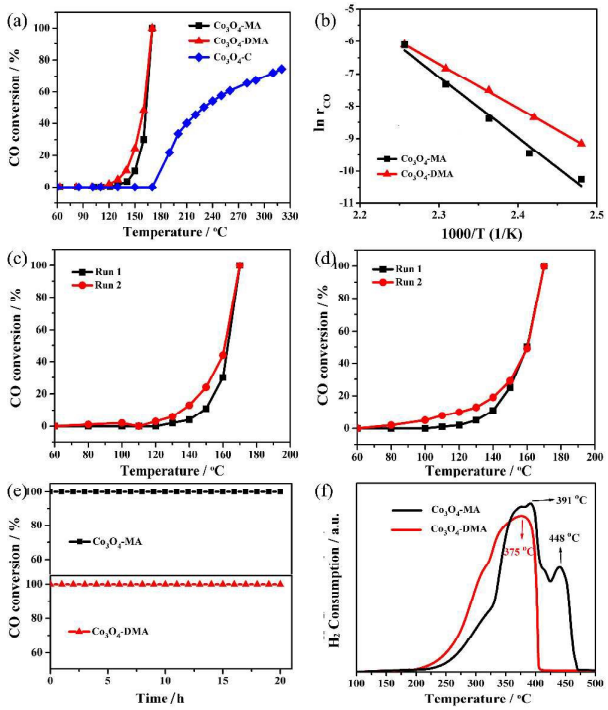

Fig. 4 (a) CO conversion curves of Co_3O_4-MA, Co_3O_4-DMA and Co_3O_4-C; (b) Arrhenius plots for the rate of CO oxidation over Co_3O_4-MA and Co_3O_4-DMA; (c) Cycling test of Co_3O_4-MA for CO conversion; (d) Cycling test of Co_3O_4-DMA for CO conversion; (e) CO conversion of Co_3O_4-MA and Co_3O_4-DMA at 180 °C with reaction time; (f) H_2-TPR profiles of Co_3O_4-MA and Co_3O_4-DMA.

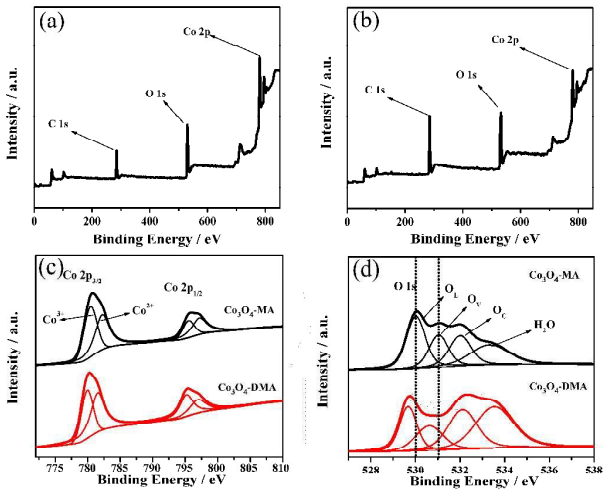

Fig. 5 XPS survey of wide scan for (a) Co_3O_4-MA and (b) Co_3O_4-DMA; XPS spectra of (c) Co 2p and (d) O 1s in Co_3O_4-MA and Co_3O_4-DMA.

View Article Online
DOI: 10.1039/C6NJ02507B

Table 1 Results of curve fitting of Co 2p and O 1s XPS spectra of the different Co_3O_4 samples

Catalyst samples	Relative percentage (%)					
	Co^{3+}	Co^{2+}	O_L [a]	O_V [b]	O_C [c]	H_2O
Co_3O_4-MA	33.7	35.7	32.2	20.3	21.9	25.6
Co_3O_4-DMA	26.8	39.3	18.6	16.4	27.5	37.5

[a] O_L = lattice oxygen. [b] O_V = oxygen vacancies. [c] O_C = chemisorbed and dissociated oxygen.

respectively, indicating the existence of cobalt, oxygen, and carbon elements in Co_3O_4-MA and Co_3O_4-DMA. The Co 2p XPS spectra profiles (Fig. 5c) are composed of two main peaks at about 780.9 eV and 796.5 eV, respectively, corresponding to the Co $2p_{1/2}$ and Co $2p_{3/2}$ spin-orbit peaks of Co_3O_4. The satellite shake-ups of Co^{2+} are located at 781.3 and 796.6 eV, and satellite shake-ups of Co^{3+} are located at 779.9 and 795.0 eV. The relative percentage of the surface-exposed Co^{3+} sites of Co_3O_4-MA is 33.7 %, which is higher than that of Co_3O_4-DMA (26.8 %), as summarized in Table 1. Unexpectedly, Co_3O_4-MA exhibits lower catalytic activity than Co_3O_4-DMA in spite of the higher superficial fraction of the Co^{3+} sites. So the components of oxygen might have effects on the catalytic reaction. Each asymmetric O 1s peak can be coherently fitted by four components, as shown in Fig. 5d. O_L component of O 1s spectra centred at 530 ± 0.2 eV, is the lattice oxygen in the Co_3O_4 phase. O_V component, centred at 531 ± 0.1 eV, is oxygen vacancies which are associated with O^{2-} ions in oxygen-deficient regions within the matrix of Co_3O_4. O_C is usually attributed to chemisorbed and dissociated oxygen species (O_2^-, O^{2-}, or O^-) and OH^- component, which is centred at around 532 ± 0.2 eV.[28, 29] The peaks at around 533 ± 0.2 eV are usually attributed to adsorbed water. Owing to lower binding energy of O_L in Co_3O_4-DMA (Fig. 5d), the O_L in Co_3O_4-DMA become more labile than that in Co_3O_4-MA, and this might be responsible for the easier generation of O_V in the Co_3O_4-DMA.[30] Furthermore, the binding energy of O_V in Co_3O_4-DMA is lower than that in Co_3O_4-MA (Fig. 5d), and this might cause O_2 molecules more easily adsorbed or desorbed in O_V sites, resulting in more active for CO oxidation of Co_3O_4-DMA.[31] The relative percentage of O_C in Co_3O_4-DMA (27.5%) is higher than that in Co_3O_4-MA (21.9%), as shown in Table 1, also suggesting that Co_3O_4-DMA exhibit more active catalytic performance. In this work, one could conclude that the synergy of O_V, O_C and Co^{3+} sites is the major possibility responsible for the high activity in CO oxidation of Co_3O_4.

4. Conclusion

In summary, we have demonstrated a novel method which employs metal-formate frameworks as precursors to prepare Co_3O_4 catalysts. As-synthesized Co_3O_4-MA and Co_3O_4-DMA with porous structures in cubic shape exhibit high activities in CO oxidation, thus display potential applications in the environmental protection. More importantly, the present work shows that pyrolysis of metal-formate frameworks is an effective and mild synthetic approaches to fabricate transition metal oxides with novel morphology and structure. The synthetic strategy can also be extended to synthesize polymetallic oxides with various mesostructures, which might possess better catalytic performance than single metal.

Acknowledgements

This work was financially supported by Key Laboratory Open Research Fund (No. 2016D03008), National Science Foundation of China (No. 21661029, U1203292, 21161020, 21301146), Natural Science Fund for Distinguished Young Scholars of Xinjiang Uygur Autonomous Region (No. 2013711008) and Technological Innovation Youth Training Project of Xinjiang Autonomous Region (No. 2013721017).

Notes and references

1 A. Alvarez, S. Ivanova, M.A. Centeno, J.A. Odriozola, *Appl. Catal. A: Gen.*, 2012, 431-432, 9-17.
2 V.M. Rao, V. Shankar, *J. Chem. Tech. Biotechnol.*, 1988, 42, 183-196.
3 X. Xie, Y. Li, Z.Q. Liu, M. Haruta, W. Shen, *Nature*, 2009, 458, 746-749.
4 K.K. Lee, W.S. Chin, C.H. Sow, *J. Mater. Chem. A,* 2014, 2, 17212-17248.
5 G. Ferey, *Chem. Soc. Rev.*, 2008, 37, 191-214.
6 J.L.C. Rowsell, O.M. Yaghi, *Micropro. Mesopor. Mater.*, 2004, 73 (1-2), 3-14.
7 J. Liu, L. Chen, H. Cui, J. Zhang, L. Zhang, C.Y. Su, *Chem Soc Rev.*, 2014, 43, 6011-6061.
8 W. Wang, Y. Li, R. Zhang, D. He, H. Liu, S. Liao, *Catal. Commun.*, 2011, **12**, 875-879.
9 Z. D. Tan, H. Y. Tan, X. Y. Shi, J. Zhuan, Y. F. Yan, Z. Yin, *Inorg. Chem. Commun.*, 2015, **61**, 128-131.
10 J. K. Sun, Q. Xu, *Energy Environ. Sci.*, 2014, **7**, 2071-2100.
11 Y. Lu, W. Zhan, Y. He, Y. Wang, X. Kong, Q. Kuang, Z. Xie, L. Zheng, *ACS Appl. Mater. Inter.*, 2014, **6**, 4186-4195.
12 K.J. Lee, T. H. Kim, T. K. Kim, J. H. Lee, H. K. Song, H. R. Moon, *J. Mater. Chem. A*, 2014, **2**, 14393-14400.
13 D.Y. Lee, S. J. Yoon, N. K. Shrestha, S. H. Lee, H. Ahn, S. H. Han, *Micropor. Mesopor. Mater.*, 2012, **153**, 163-165.
14 J. Y. Ye, C. J. Liu, *Chem. Comm,* 2011, 47, 2167-2169.
15 S. Zhang, H. Liu, C. Sun, P. Liu, L. Li, Z. Yang, X. Feng, F. Huo, X. Lu, *J. Mater. Chem. A*, 2015, **3**, 5294-5298.
16 Y. H. Qin, L. Huang, D. L. Zhang, L. G. Sun, *Inorg Chem Commun*, 2016, **66**, 64-68.
17 N. Yan, Q. Chen, F. Wang, Y. Wang, H. Zhong, L. Hu, *J. Mater. Chem. A*, 2013, **1**, 637-643.
18 X. Wang, W. Zhong, Y. Li, *Catal. Sci. Technol.,* 2015, **5**, 1014-1020.
19 H. Pang, F. Gao, Q. Chen, R. Liu, Q. Lu, *Dalton. Trans*, 2012, **41**, 5862-5868.
20 K. L. Hu, M. Kurmoo, Z. M. Wang, S. Gao, *Chem.- A Eur. J.*, 2009, **15**, 12050-12064.
21 Z. M. Wang, B. Zhang, T. Otsuka, K. Inoue, H. Kobayashi, M. Kurmoo, *Dalton. Trans.*, 2004, 2209-2216.
22 Z. M. Wang, K. L. Hu, S. Gao, H. Kobayashi, *Adv Mater,* 2010, **22**, 1526-1533.
23 B. Meng, Z. Zhao, X. Wang, J. Liang, J. Qiu, *Appl. Catal. B: Environ.*, 2013, **129**, 491-500.
24 J. Luo, M. Meng, X. Li, X. Li, Y. Zha, T. Hu, Y. Xie, J. Zhang, *J. Catal.*, 2008, **254**, 310-324.
25 F. Wang, X. Wang, D. Liu, J. Zhen, J. Li, Y. Wang, H. Zhang, *ACS Appl. Mater. Inter.,* 2014, **6**, 22216-22223.
26 H. Zhang, X. Hu, *Sep. Purif. Technol.*, 2004, **34**, 105-108.
27 Y. B. Yu, T. Takei, H. Ohashi, H. He, X. L. Zhang and M. Haruta, *J. Catal.*, 2009, **267**, 121-128.
28 Z. Wu, R. Jin, Y. Liu, H. Wang, *Catal. Commun.* 2008, **9**, 2217-2220.
29 M. Kang, E. D. Park, J. M. Kim, J. E. Yie, *Appl. Catal. A: Gen.*, 2007, **327**, 261-269.
30 P. Sudarsanam, B. Mallesham, D. N. Durgasri, B.M. Reddy, *RSC Advances,* 2014, **4**, 11322-11330.
31 W. Song, A.S. Poyraz, Y. Meng, Z. Ren, S.-Y. Chen, S.L. Suib, *Chem. Mater.*, 2014,**26**, 4629-4639.